



HAL
open science

Revisiting the mesoscopic Termonia and Smith model for deformation of polymers

B. Krishna Reddy, Rafael Estevez, Sumit Basu

► **To cite this version:**

B. Krishna Reddy, Rafael Estevez, Sumit Basu. Revisiting the mesoscopic Termonia and Smith model for deformation of polymers. *Modelling and Simulation in Materials Science and Engineering*, 2008, 16 (2), pp.025008. 10.1088/0965-0393/16/2/025008 . hal-01815411

HAL Id: hal-01815411

<https://hal.science/hal-01815411>

Submitted on 6 Apr 2023

HAL is a multi-disciplinary open access archive for the deposit and dissemination of scientific research documents, whether they are published or not. The documents may come from teaching and research institutions in France or abroad, or from public or private research centers.

L'archive ouverte pluridisciplinaire **HAL**, est destinée au dépôt et à la diffusion de documents scientifiques de niveau recherche, publiés ou non, émanant des établissements d'enseignement et de recherche français ou étrangers, des laboratoires publics ou privés.



Distributed under a Creative Commons Attribution - NonCommercial 4.0 International License

Revisiting the mesoscopic Termonia and Smith model for deformation of polymers

B Krishna Reddy¹, Rafael Estevez² and Sumit Basu¹

¹ Department of Mechanical Engineering, Indian Institute of Technology Kanpur, Kanpur 208016, UP, India

² INSA Lyon, MATEIS, Av A Einstein, Bât. St Exupéry, 69621 Villeurbanne Cedex, France

Abstract

Mesoscopic models for polymers have the potential to link macromolecular properties with the mechanical behaviour without being too expensive computationally. An interesting, popular and rather simple model to this end was proposed by Termonia and Smith (1987 *Macromolecules* **20** 835–8). In this model the macromolecular ensemble is viewed as a collection of two-dimensional self-avoiding random walks on a regular lattice whose lattice points represent entanglements. The load is borne by members representing van der Waals bonds as well as macromolecular strands between two entanglement points. Model polymers simulated via this model exhibited remarkable qualitative similarity with real polymers with respect to their molecular weight, entanglement spacing, strain rate and temperature dependence. In this work, we revisit this model and present a detailed reformulation within the framework of a finite deformation finite element scheme. The physical origins of each of the parameters in the model are investigated and inherent assumptions in the model which contribute to its success are critically probed.

1. Introduction

Suitably designed mesoscopic models for the deformation and fracture of solid polymers form an important bridge between atomistic and continuum models. Atomistic methods such as molecular dynamics (MD) (e.g. Brown and Clarke 1991, Capaldi *et al* 2004, Negi and Basu 2006) can simulate deformation behaviour at very high strain rates on nanoscopic specimens. On the other hand, continuum methods (e.g. Boyce *et al* 1988, Wu and van der Giessen 1993) can model mechanical behaviour at macroscopic scales but are phenomenological in nature and as a result cannot directly establish connections between microscopic properties (such as molecular weight of the macromolecule) and macroscopic mechanical properties.

A simple lattice model for simulating the deformation and fracture of solid polymers has been proposed by Termonia and Smith (1987, 1988) and Termonia *et al* (1988). Henceforth we will refer to this as the TS model. This model treats entanglements between polymer chains as unbreakable (though in another version of the model slip of macromolecular chains through entanglement points and consequent occasional disentanglement is allowed) and a chain is thought of as being a self-avoiding random walk (SARW) through a regular grid of entanglement points. The portions of a chain between two entanglement points, called ‘strands’, behave as rubber elastic springs governed by the inverse Langevin function (Treloar 1975). Additionally, the non-bonded van der Waals interaction between the chains is represented by discrete linear elastic members. In the original model, both the van der Waals elements and the ‘strand’ elements can break leading to a loss in the stress carrying capacity of the material. Breakage rules for the van der Waals members are motivated by kinetic theory of fracture and the members are broken through a Monte Carlo lottery. Thus the breakage rule depends on a critical stress though no length scale characteristic of the mesh is included (Curtin and Scher 1990, Jagota and Bennisson 1995). Models similar in spirit to the TS model have been used to deal with time dependent damage evolution (Curtin and Pamel 1997, Vujosevic and Krajcinovic 1997) and fracture of fibres (Gonzalez and Llorca 2003). Recently, variants of the Termonia and Smith model incorporating slippage of chains through entanglements have been used by Terzis *et al* (2002) to study the deformation and fracture of bi-polymeric interfaces.

The original TS papers concentrated on the behaviour of polyethylene at high temperatures ($>100\text{ }^{\circ}\text{C}$) but the modelling methodology is essentially applicable to even amorphous polymers in the glassy state. This is due to the fact that the stress–strain response predicted by the model for semi-crystalline polyethylene has qualitative features that resemble the behaviour of a range of polymers under a range of conditions. Comparison of the predictions from the TS model with experimental stress–strain behaviours of a number of commercial polymers has been performed by Bicerano *et al* (1997). The results for amorphous polymers showed good quantitative agreement with atactic polystyrene and ethylene–propylene–diene terpolymers at a range of temperatures.

Though the TS model is simple in principle, a systematic evaluation of the significance of the various parameters involved in the model has not been performed. In this work we present a clearly formulated finite element based numerical model for a two-dimensional polymer represented by SARWs on a lattice of entanglement points. The method adopted in this paper to deform the macromolecular ensemble is significantly different from that used by Termonia and Smith (1987) and Bicerano *et al* (1997). The method is based on the realization that the macromolecular ensemble is basically a two-dimensional truss-like structure amenable to a non-linear finite element analysis, where the individual members (the strands and the van der Waals members) can undergo large deformations and rotations. In this regard, the numerical algorithm used is similar in spirit to the rod finite elements adopted by Gonzalez and Llorca (2003).

The TS model is able to reproduce the uniaxial stress–strain behaviour of polymers qualitatively. We show that the reason for this success lies in a changeover in the load bearing behaviour of the network with strain. In other words, the energetics of the network shift from being van der Waals dominated at low strains to rubber elasticity dominated at higher strains. Thus, parametrization of the discrete van der Waals members vis-a-vis the rubber elastic behaviour of the chains is the key to fitting the simulated results to the experimental ones. To this end, we take the parameters presented in the original papers as a basis and explore, through a systematic parametric study, the influence of the key parameters on the overall stress–strain response.

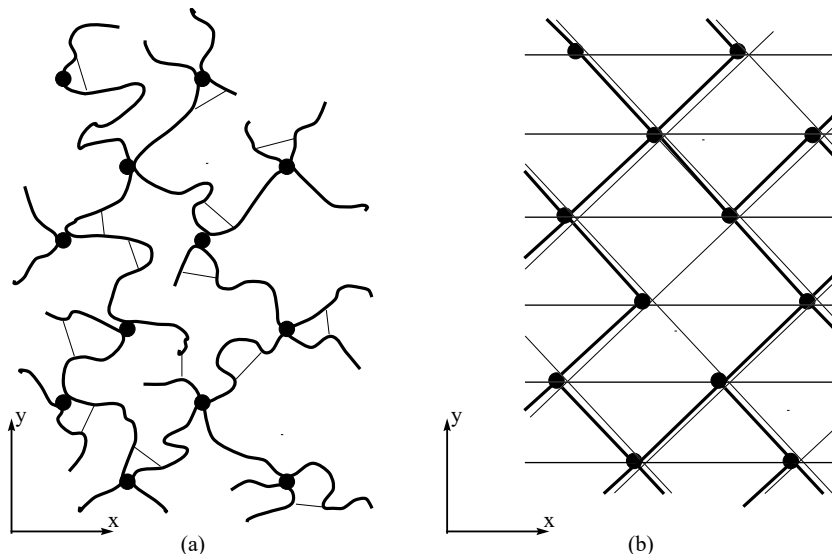


Figure 1. Schematic showing the two-dimensional TS idealization in (b) of an actual dense macromolecular system shown in (a).

This paper is organized in the following way. The next section describes the sample generation procedure, the finite element solution method and techniques used for breaking the van der Waals bonds and the macromolecular chains. In section 3 the influence of various model parameters is discussed. Conclusions and discussions on the efficacy of the present method are presented in section 4.

2. Computational procedure

The computational procedure consists of a few basic steps. First, a regular lattice of entanglement points (also called nodes) is filled up with SARWs of a given length N such that two and only two SARWs pass through each node. These SARWs represent macromolecular chains. Superposed on this ensemble is a regular lattice of van der Waals members obeying linear elasticity. The second step is to perform a finite element analysis of this two-dimensional structure under volume preserving uniaxial stretching at a particular rate. The finite element assemblage is composed of non-linear (strand elements) and linear (van der Waals members) truss elements. During deformation, both van der Waals bonds and the macromolecular chains can break leading to loss of stiffness. The analysis is stopped when the sample is separated into two parts.

2.1. Sample preparation

Figure 1(a) is a schematic showing the situation prevailing in a real polymer. The heavy black circles represent entanglements between the coiled polymer chains and the dotted lines denote the van der Waals bonds acting between different parts of a chain as well as between neighbouring chains. In figure 1(b) is shown the idealized TS model (Termonia and Smith 1987). The heavy solid lines indicate chain vectors between entanglements and the individual van der Waals bonds have been replaced by discrete members

(dotted lines) joining each entanglement to its nearest neighbours. In the TS model, the chains start or end at an entanglement point since loose chain ends do not bear any load and are thus superfluous in the present context.

The chain vectors in an actual, undeformed specimen are randomly oriented in a three-dimensional space, i.e. $\langle \cos^2 \psi \rangle = \frac{1}{3}$, where ψ is the vector's angle with the draw axis y . In our simplified, regular two-dimensional representation (figure 1(b)), we have taken all strands to be oriented at $\psi = 54.7^\circ$ with the x -axis. We should note here that the TS model also used a similar orientation though in two-dimensions this does not lead to a strand that has equal orientation to both the axes. A value of $\psi = 45^\circ$ is probably more suitable in two-dimensions. However, we found that the effect of the strand orientations on the overall results to be presented later is small and we have adopted $\psi = 54.7^\circ$ to be consistent with the TS model.

The simplified model is generated with the following considerations.

- (i) Each chain behaves like a SARW and thus a chain does not cross itself.
- (ii) One chain does not overlap with another, i.e. no two chains have the same two consecutive entanglement points.
- (iii) Chains do not cross each other.
- (iv) Periodic boundary conditions apply in the x direction.

Ideally, the chain generation process stops after all entanglement points have been visited by two and only two chains. However, this may not always be possible satisfying all the above conditions (i)–(iv). Several trials may be required before a suitable sample is generated.

Selection of a suitable generation procedure for a single chain in a dense system is important for achieving complete occupancy of the lattice. We are interested in rather short SARWs (of 5–10 steps each) and so we adopt a simple algorithm suggested by Sokal (1995) for generating a single chain. It should be noted that more sophisticated schemes for single chain generation have been used for generating dense fully occupied systems by Meirovitch (1987) and Mansfield (1982) among others. However, for the short length SARWs that we use, the algorithm due to Sokal (1995) turns out to be adequate in the sense that it yields an almost monodisperse ensemble with all entanglement points occupied by two and only two chains.

Polymers live in three-dimensional spaces. The two-dimensional lattice used here is at best an approximation. The two-dimensional polymer sheet analysed can be thought of as being one out of an infinite number of sheets arranged like a stack of cards. This stack makes up the actual three-dimensional sample. Entanglements between chains are also basically three-dimensional entities and in two-dimensions are represented as nodes at which two self-avoiding walks are connected. The distance between the sheets at the onset in the z direction is given by T_0 . When the system is stretched in the y direction, it contacts in the other directions and consequently the distance between the sheets is also reduced. Assumptions used in determining T_0 are discussed in section 2.5.

Figure 2 shows the chain length distributions in the whole sample after filling it up with multiple strands. Some chains need to be truncated at the top and bottom surfaces of the domain while a few chains (especially when most of the system is filled up) cannot be grown to their desired length because of overcrowding. Both these contribute to the fact that the average chain length p_{avg} falls below the desired length p . In figure 2, the horizontal axis represents the size M of the $M \times M$ grid used. For the number of strands in a chain $p = 1, 5, 10$ and 15 , we are able to generate $p_{\text{avg}} = 1, 4.3, 7.3$ and 8.2 , respectively. Also there is very little effect of M on the value of p_{avg} . The polydispersity is somewhat high for SARW sizes greater than 5 steps produced with our simple algorithm for generating dense systems. For the

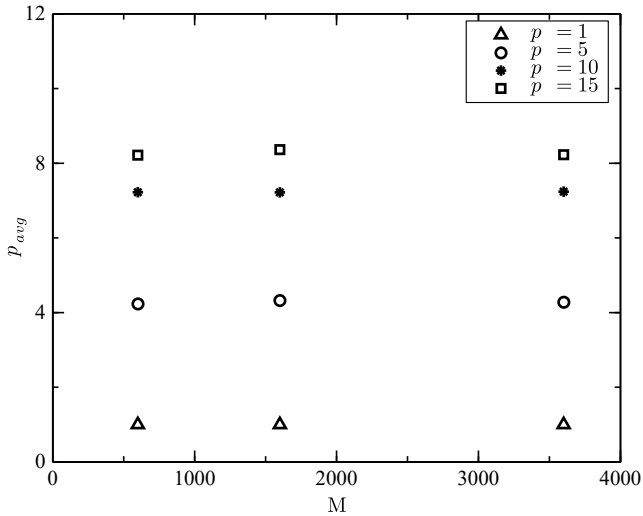


Figure 2. Average chain lengths p_{avg} of dense samples obtained using $M \times M$ meshes. The desired chain lengths are given by p .

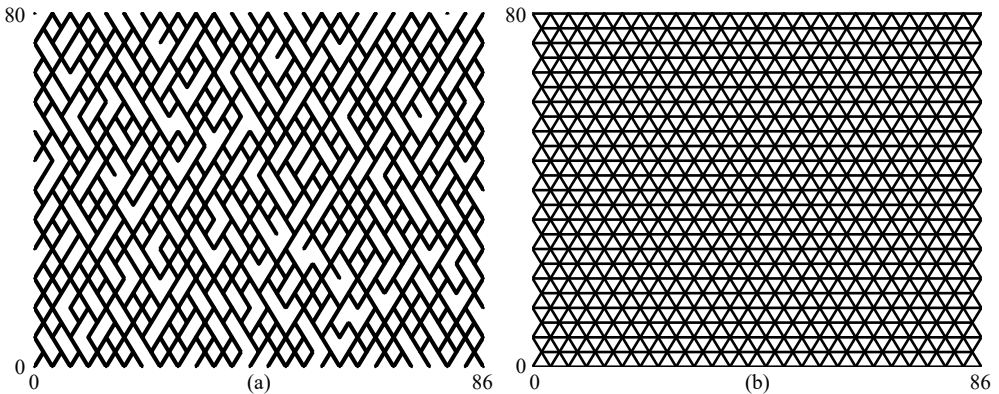


Figure 3. A small 25×25 grid showing (a) a mesh with strand elements as part of 5 step SARWs and (b) only van der Waals members.

model macromolecules considered in this study, a 5 step SARW represents a chain with about 700 monomers³.

The mesoscopic model of the polymer is obtained by taking into consideration both van der Waals bonds and the strands. This is shown in figures 3(a) and (b) for a small 25×25 grid containing 100 chains with $p = 5$. Figure 3(a) shows a sample with only the macromolecular strands. Each strand connecting two entanglement points is assumed to follow inverse Langevin based rubber elasticity (Treloar 1975). The van der Waals force acting between neighbouring atoms is lumped into a network of linear, breakable springs joining entanglement points and forming a regular two-dimensional triangular lattice as shown in figure 3(b). The final model consists of the triangular lattice (shown in figure 3(b)) superposed on the ensemble of SARWs representing the macromolecules in figure 3(a).

³ Assuming, as in the original TS paper, that each step comprises 14 Kuhn segments or strands per step and that each strand is made up of about 10 monomers.

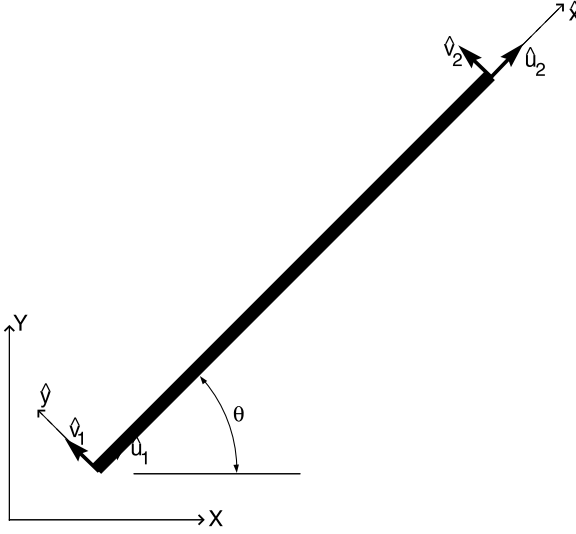


Figure 4. A typical rod element used in this work. The symbols used are defined in the text.

2.2. Finite element formulation for the assemblage

As mentioned earlier, the generated sample consists of non-linear members formed by the strands and linear van der Waals members. Under uniaxial stretching, the members can undergo large rotations and deformations.

In the finite element model we consider the general case of a truss member whose stiffness is a sum total of the stiffnesses of an inverse Langevin and a linear spring. Within the assemblage, a particular member may have either or both of these two contributions active at a point of time. Here we discuss the corotational formulation for such a general truss element.

We start with the equation of virtual power in terms of first Piola Kirchhoff stress \mathbf{P} in the absence of body forces and surface tractions. Thus,

$$\int_{V_0} \mathbf{P} : \delta \dot{\mathbf{F}} dV_0 = 0, \quad (1)$$

where \mathbf{F} is the deformation gradient tensor and for two second order tensors \mathbf{A} and \mathbf{B} , $\mathbf{A} : \mathbf{B} = A_{ij} B_{ji}$. In terms of the Cauchy stress $\boldsymbol{\sigma}$, using $\mathbf{P} = J\mathbf{F}^{-1}\boldsymbol{\sigma}$, \mathbf{L} as the velocity gradient tensor with \mathbf{D} as its symmetric part and $J = \det(\mathbf{F})$, we can write for volume preserving deformations (i.e. $\dot{J} = 0$)

$$\dot{\mathbf{P}} = J\mathbf{F}^{-1}(\dot{\boldsymbol{\sigma}} - \mathbf{L}\boldsymbol{\sigma}).$$

Thus, the incremental form of equation (1), namely, $\int_{V_0} \dot{\mathbf{P}} : \delta \dot{\mathbf{F}} dV_0 = 0$, in the deformed configuration becomes

$$\int_V \delta \mathbf{L} : [\dot{\boldsymbol{\sigma}} - \mathbf{L}\boldsymbol{\sigma}] dV = 0, \quad (2)$$

where $\delta \mathbf{L} = \delta \dot{\mathbf{F}}\mathbf{F}^{-1}$.

Now consider a one-dimensional 2-node truss element with a corotational axis \hat{x} having a current cross sectional area A and a current length l (see figure 4). For a volume preserving

deformation of this bar, along \hat{x} , the virtual power equation simplifies to

$$\int_V \delta \hat{D}_{\hat{x}\hat{x}} (\hat{\sigma} - \hat{D}_{\hat{x}\hat{x}} \hat{\sigma}_{\hat{x}\hat{x}}) A \, d\hat{x} = 0,$$

where $(\hat{\cdot})$ denotes quantities in the \hat{x} coordinate system.

For the 2-node bar, the velocities \hat{u} and \hat{v} are interpolated in terms of their nodal values as

$$\hat{u} = N_1 \hat{u}_1 + N_2 \hat{u}_2 \quad \text{and}$$

$$\hat{v} = N_1 \hat{v}_1 + N_2 \hat{v}_2,$$

where $N_1 = 1 - \hat{x}/l$, and $N_2 = \hat{x}/l$. Thus,

$$\hat{D}_{\hat{x}\hat{x}} = \begin{bmatrix} -1 & 0 & 1 & 0 \end{bmatrix} \begin{Bmatrix} \hat{u}_1 \\ \hat{v}_1 \\ \hat{u}_2 \\ \hat{v}_2 \end{Bmatrix} = \hat{\mathbf{B}} \hat{\mathbf{u}}. \quad (3)$$

This immediately leads to

$$\int_V \delta \hat{\mathbf{u}}^T \hat{\mathbf{B}}^T [\hat{\sigma}_{\hat{x}\hat{x}} - \hat{\mathbf{B}} \hat{\mathbf{u}} \hat{\sigma}_{\hat{x}\hat{x}}] A \, d\hat{x} = 0. \quad (4)$$

In general an element supports two types of forces. The total force \hat{f} on an element is given by

$$\hat{f} = \hat{f}_s(\lambda) + \hat{f}_{vd}(\lambda), \quad (5)$$

where \hat{f}_s is the ‘strand force’ arising out of the non-linear spring character of the strand and \hat{f}_{vd} is the van der Waals force. The quantity λ is the instantaneous stretch. Therefore

$$\dot{\hat{f}} = \hat{f}'_s \dot{\lambda} + \hat{f}'_{vd} \dot{\lambda}. \quad (6)$$

The force on any member in the \hat{x} direction is given by

$$\hat{f} = \hat{\sigma}_{\hat{x}\hat{x}} A, \quad (7)$$

where A is the current area of the member, whereby,

$$\dot{\hat{f}} = \dot{\hat{\sigma}}_{\hat{x}\hat{x}} A + \hat{\sigma}_{\hat{x}\hat{x}} \dot{A}. \quad (8)$$

Using volume conservation the area and length in the reference configuration A_0 and l_0 can be related to A and l as $A_0 l_0 = A l$. The fact that the volume of each ‘strand’ element is conserved follows from the picture of the element that we have in mind. The radius of each element in the undeformed state is equal to $r_{g\perp}$, the component of the radius of gyration perpendicular to the Gaussian end to end vector \mathbf{R}_{ee} . When the element is stretched uniaxially to λR_{ee} , $r_{g\perp}$ scales as $1/\sqrt{\lambda}$ (see, Heymans (1988)). This implies volume conservation and we get

$$\dot{\hat{f}} = \dot{\hat{\sigma}}_{\hat{x}\hat{x}} \frac{A_0}{\lambda} - \frac{\hat{\sigma}_{\hat{x}\hat{x}} A_0}{\lambda^2} \dot{\lambda}, \quad (9)$$

where $\lambda = l/l_0$. Using equation (6) in the LHS of equation (9) we get

$$\hat{f}'_s \dot{\lambda} + \hat{f}'_{vd} \dot{\lambda} = \dot{\hat{\sigma}}_{\hat{x}\hat{x}} \frac{A_0}{\lambda} - \frac{\hat{\sigma}_{\hat{x}\hat{x}} A_0}{\lambda^2} \dot{\lambda}, \quad (10)$$

leading to

$$\dot{\hat{\sigma}}_{\hat{x}\hat{x}} = \frac{\lambda}{A_0} \left[\hat{f}'_s + \hat{f}'_{vd} + \frac{\hat{\sigma}_{\hat{x}\hat{x}} A_0}{\lambda^2} \right] \dot{\lambda} = \frac{\lambda}{A_0} C(\lambda) \dot{\lambda}, \quad (11)$$

where $C(\lambda) = f'_s + f'_{vd} + \hat{\sigma}_{\hat{x}\hat{x}} A_0 / \lambda^2$. It can be easily shown that

$$\dot{\lambda} = \lambda \hat{\mathbf{B}} \hat{\mathbf{u}}. \quad (12)$$

Using equation (12) in (11), then inserting in equation (4) and using the usual finite element procedures yield

$$\hat{\mathbf{K}} \hat{\mathbf{u}} = 0, \quad \hat{\mathbf{K}} = \hat{\mathbf{K}}_{\text{mat}} + \hat{\mathbf{K}}_{\text{geo}}, \quad (13)$$

where \mathbf{K}_{mat} is the material stiffness matrix and \mathbf{K}_{geo} is the geometric stiffness matrix. Further,

$$\hat{\mathbf{K}}_{\text{mat}} = \int_V \hat{\mathbf{B}}^T \frac{\lambda}{A_0} C(\lambda) \lambda \hat{\mathbf{B}} dV. \quad (14)$$

When written explicitly this becomes

$$\hat{\mathbf{K}}_{\text{mat}} = \frac{\lambda^2}{A_0} C(\lambda) \begin{pmatrix} 1 & 0 & -1 & 0 \\ 0 & 0 & 0 & 0 \\ -1 & 0 & 1 & 0 \\ 0 & 0 & 0 & 0 \end{pmatrix}. \quad (15)$$

Moreover, using the definition of $\hat{\mathbf{B}}$, it is easy to show that the expression for the geometric stiffness matrix is

$$\hat{\mathbf{K}}_{\text{geo}} = -\frac{\hat{\sigma}_{\hat{x}\hat{x}} A}{l} \begin{pmatrix} 1 & 0 & -1 & 0 \\ 0 & 0 & 0 & 0 \\ -1 & 0 & 1 & 0 \\ 0 & 0 & 0 & 0 \end{pmatrix}. \quad (16)$$

The stiffness matrices in the (\hat{x}, \hat{y}) system \mathbf{K}_{mat} and \mathbf{K}_{geo} can be easily transformed to the global (X, Y) system through

$$\begin{aligned} \mathbf{K}_{\text{mat}} &= \mathbf{T}^T \hat{\mathbf{K}}_{\text{mat}} \mathbf{T} \quad \text{and} \\ \mathbf{K}_{\text{geo}} &= \mathbf{T}^T \hat{\mathbf{K}}_{\text{geo}} \mathbf{T}, \end{aligned} \quad (17)$$

where the transformation matrix \mathbf{T} is given by

$$\mathbf{T} = \begin{pmatrix} \cos \theta & \sin \theta & 0 & 0 \\ -\sin \theta & \cos \theta & 0 & 0 \\ 0 & 0 & \cos \theta & \sin \theta \\ 0 & 0 & -\sin \theta & \cos \theta \end{pmatrix}. \quad (18)$$

Therefore, in the global (X, Y) system we have in terms of the angle θ the bar which it makes with the X axis (see figure 4),

$$\mathbf{K}_{\text{mat}} = \frac{\lambda^2}{A_0} C(\lambda) \begin{pmatrix} \cos^2 \theta & \cos \theta \sin \theta & -\cos^2 \theta & -\cos \theta \sin \theta \\ \cos \theta \sin \theta & \sin^2 \theta & -\cos \theta \sin \theta & -\sin^2 \theta \\ -\cos^2 \theta & -\cos \theta \sin \theta & \cos^2 \theta & \cos \theta \sin \theta \\ -\cos \theta \sin \theta & -\sin^2 \theta & \cos \theta \sin \theta & \sin^2 \theta \end{pmatrix}. \quad (19)$$

The geometric stiffness is invariant to rotation and thus

$$\mathbf{K}_{\text{geo}} = -\frac{f_s + f_{vd}}{l} \begin{pmatrix} 1 & 0 & -1 & 0 \\ 0 & 1 & 0 & -1 \\ -1 & 0 & 1 & 0 \\ 0 & -1 & 0 & 1 \end{pmatrix}. \quad (20)$$

The total stiffness in the global (X, Y) system is given by the sum of the material and geometric stiffnesses as

$$\mathbf{K} = \mathbf{K}_{\text{mat}} + \mathbf{K}_{\text{geo}}. \quad (21)$$

According to classical theory of rubber elasticity for non-Gaussian chains, force on a chain strand having a vector length r is given by (see Treloar (1975))

$$\hat{f}_s = \frac{kT}{l_s} \mathcal{L}^{-1} \left(\frac{r}{Nl_s} \right), \quad (22)$$

where N is the number of statistical chain segments (Kuhn segments) and l_s is their length. The inverse Langevin function \mathcal{L}^{-1} for an arbitrary variable s can be approximated as (see Perrin (2000))

$$\mathcal{L}^{-1}(s) = \frac{s(3 - s^2)}{(1 - s^2)}. \quad (23)$$

Thus equation (22) becomes

$$\hat{f}_s = \frac{kT}{l_s} \frac{\hat{\lambda}}{\sqrt{N}} \left[\frac{(3N - \hat{\lambda}^2)}{N - \lambda^2} \right] \quad (24)$$

and

$$\hat{f}'_s = \frac{kT}{l_s} \frac{1}{\sqrt{N}} \left[\frac{3(N - \lambda^2)^2 + 2\lambda^2(3N - \lambda^2)}{(N - \lambda^2)^2} \right]. \quad (25)$$

Further, the van der Waals force is assumed to lead to a linear elastic stress–stretch relationship and

$$\hat{f}_{\text{vd}} = K_{\text{vd}} A_{\text{vd}} \left(1 - \frac{1}{\lambda} \right), \quad (26)$$

where K_{vd} is the elastic modulus. The area of the van der Waals member in the reference configuration is A_{vd} , which is equal to A when the van der Waals member overlaps a strand. A different area is used for the horizontal van der Waals members which do not overlap with strand elements. Issues regarding estimation of K_{vd} and A_{vd} are discussed later. Thus,

$$f'_{\text{vd}} = \frac{K_{\text{vd}} A_{\text{vd}}}{\lambda^2}. \quad (27)$$

Therefore the non-linear finite element problem can now be solved in principle with velocities applied at specific nodes.

2.3. Boundary conditions

The geometry chosen for analysis is as shown in figure 5. We start with a unit cell of dimension $B_0 \times H_0 \times T_0$ that deforms in a volume preserving way to a cell of dimensions $B \times H \times T$ at time t . The boundary conditions in terms of the velocity components u and v applied on the edges of the unit cell are

$$\begin{aligned} u(0, y, t) &= 0 & \text{and} \\ v(x, 0, t) &= 0. \end{aligned} \quad (28)$$

In addition, at any point of time t

$$\begin{aligned} v(x, H, t) &= v_0 & \text{and} \\ u(y, B, t) &= u_0(t). \end{aligned} \quad (29)$$

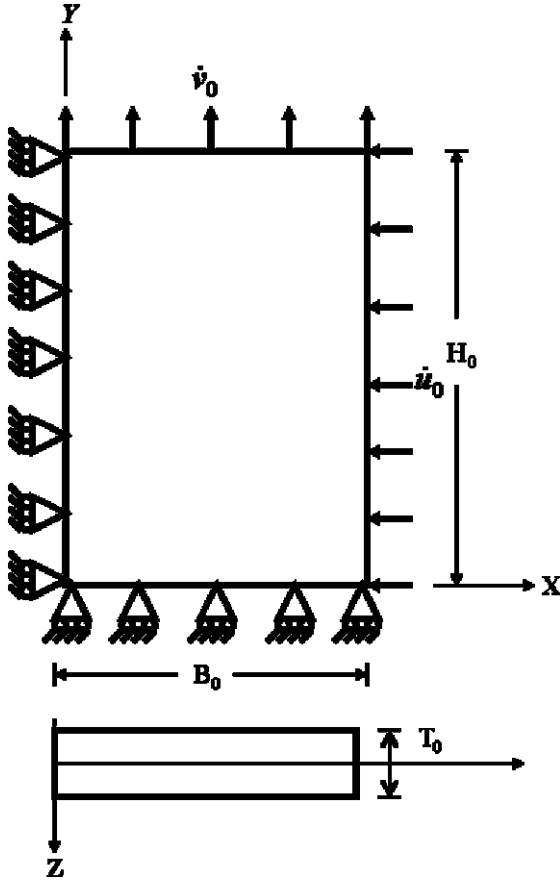


Figure 5. Schematic showing the problem analysed in this work and the applied boundary conditions. The quantity v_0 is the constant velocity applied at the top face while i_0 is the appropriate velocity applied on the right face in order to keep the volume of the unit cell constant.

In the above, the velocity of the top face v_0 is kept constant. Furthermore, in order to perform the analysis at constant volume, at any point of time we need to have the principal stretches in the y and x directions related as

$$\lambda_x = \frac{1}{\sqrt{\lambda_y}}.$$

This can be achieved if

$$u_x(t) = -\frac{v_0}{2\lambda_y^{\frac{3}{2}}} \frac{B_0}{H_0} \quad \text{in equation (29).}$$

The overall strain E_y is defined as

$$E_y(t) = \frac{v_0 t}{H}. \quad (30)$$

The overall stress Σ_y is obtained from

$$\Sigma_y = \frac{1}{V} \frac{\partial U}{\partial E_y}, \quad (31)$$

where U is the total strain energy stored in the unit cell.

The unit cell also has a thickness T_0 such that only a single polymeric layer is enclosed in the cell. The initial thickness T_0 is assumed to be equal to the distance between the entanglement points $\sqrt{N}l_s$, which equals the Gaussian end to end distance for a chain of length N . Thus, plane stress conditions are assumed to prevail where the thickness of the unit cell scales as $T = T_0\lambda_y^{-1/2}$.

2.4. Sources of irreversibility

As the system of entangled polymeric chains analysed here is deformed, two debilitating processes occur. They are the breakage of van der Waals bonds and scission of the macromolecular chains. As in Termonia and Smith (1987) van der Waals bonds break according to kinetic theory of fracture at the rate

$$\nu = \tau \exp\left[-\frac{(U_0 - \beta\hat{\sigma})}{k_B T}\right]. \quad (32)$$

Here τ is the thermal vibration frequency and U_0 and β are the activation energy and volume, respectively. Also k_B is Boltzmann's constant and T is the temperature.

The simulation of van der Waals bond breaking is performed with the help of a Monte Carlo lottery that continues with a pre-set time step of Δt till a desired strain level E_y is attained. At every time step, the calculations proceed in the following manner.

1. Apply a displacement increment $v_0\Delta t$ on the top face at $y = H$ and the corresponding volume preserving displacements at the right edge $x = B$.
2. Solve the finite element system for the displacement increments applied in step 1 to obtain new displacements of all nodes and forces in all elements.
3. Start the bond breaking process. Initialize $\zeta = 0$.
4. Calculate a probability

$$P_i = \frac{\nu_i}{\nu_{\max}}, \quad (33)$$

where ν_i and ν_{\max} are the rates of breaking of the i th and the most strained bond in the ensemble.

5. Within the analysis time step Δt , visit the intact van der Waals bonds at random.
6. Generate a uniformly distributed random number R_i on a visit to bond i .
7. Break bond i if $R_i < P_i$, else go to the next bond.
8. After each visit of a bond ζ is incremented by $1/[\nu_{\max}n_{\text{vd}}(t)]$, where $n_{\text{vd}}(t)$ is the total number of intact bonds at time t .
9. Terminate the process, increment time by Δt and go back to step 1 when $\zeta \geq \Delta t$.

Additionally, in view of equation (23) it is evident that as the value of $s \rightarrow 1$ the force $\hat{f}_s \rightarrow \infty$. We therefore break a strand when the draw ratio of a strand approaches \sqrt{N} .

In Washiyama *et al* (1993), the minimum force required to cause scission of a polymeric chain is estimated to be around 2 nN. In our case, for a strand with $N = 14$, at $T = 300$ K, this would imply a stretch in the strand of the order $\lambda \simeq 0.99\sqrt{N}$. Thus, the probability of a strand breaking at lower stretches is negligibly small and unlike the van der Waals bonds, the strand breakage rule is assumed to be deterministic: a strand breaks when it attains a stretch of \sqrt{N} .

The inherent assumption in the TS model therefore is that plasticity in polymers stems from the breaking of van der Waals bonds and scission of polymer chains. The TS model considers chain slippage and consequent disentanglement as possible additional sources of irreversibility. However, at low temperatures in the glassy regime disentanglement seems less likely compared with the mechanisms considered here.

2.5. Parameters

Several parameters are involved in the TS model. The most important parameters pertain to equation (32). In this work, following the original paper (Termonia and Smith 1987), we define a ‘base’ material for which the parameters are the same as in the TS model, i.e. $U_0 = 1.9 \times 10^{-19}$ J, $\tau = 10^{12}$ s $^{-1}$ and $\beta = 1.75 \times 10^{-26}$ m 3 . In equation (22), the number of statistical segments per strand is $N = 14$ with each segment being $l_s = 10$ Å in length.

The simulations were conducted at $T = 473$ K unless otherwise mentioned. However, the exact value of the temperature is not very important (except to compare with the TS results) for our purpose since experimental uniaxial deformation behaviour at any other lower temperature can be fitted by a proper choice of parameters.

The van der Waals members have stiffness $K_{vd} = 4$ MPa. There are two kinds of discrete van der Waals members in the assemblage. There are van der Waals members overlapping with the strand elements and horizontal ones. The horizontal van der Waals members have a cross sectional area $A_{vd} = 2Nl_s^2 \cos \theta$ representing in a lumped manner the integrated non-bonded interaction between the neighbouring chains.

The overlapping van der Waals members and the strands have the same cross sectional area $A_0 = \pi r_{g\perp}^2 l_s$, assuming that these members are cylindrical rods having radii equal to the component of the radius of gyration $r_{g\perp}$ perpendicular to the strand axis. Assuming that the strand is randomly coiled at the onset, $r_{g\perp} = \sqrt{1/3} \sqrt{N/6} l_s$ under the Gaussian approximation (see Treloar (1975)). The van der Waals forces along the strands represent the lumped effect of the intrachain non-bonded interactions. We use ~ 10000 nodes (entanglement points) in our simulations representing an initial box size of about 0.8×0.8 μm^2 .

3. Results and discussions

In this section we present and discuss salient results from uniaxial deformation of the ‘base’ material. In particular we focus on the physical significance of the parameters involved in the TS model. The objective is to try and understand the inherent assumptions in the model so that at a later stage parameters for it can be derived from lower order simulations such as MD.

3.1. Significance of various parameters in the TS model

In figures 6(a)–(c), we illustrate the behaviour of the ‘base’ material as it is strained. In figure 6(a), the evolution of the number of intact van der Waals bonds n_{vd} (normalized with n_{vd0} , the number of intact bonds at $E_y = 0$) with the overall strain E_y is demonstrated. Clearly, most van der Waals bonds break within the early part of the deformation. Beyond $E_y = 2$ no more van der Waals bonds break and the load is borne primarily by the strands. The transfer of load from the van der Waals bonds to the polymer strands manifest as a point of inflection on the total energy U versus E_y curve shown in figure 6(b). The total energy is calculated by summing the strain energies of all elements in the system as

$$U(E_y) = \sum_i \int_1^{\lambda_i} \hat{f}_s^i l_0^i d\lambda_i + \int_1^{\lambda_i} \hat{f}_{vd}^i l_0^i d\lambda_i. \quad (34)$$

In the above equation, \hat{f}_s^i and \hat{f}_{vd}^i denote the strand and van der Waals forces on the element i , while l_0^i is its initial length. The quantity λ_i is the stretch in element i when the overall strain is E_y .

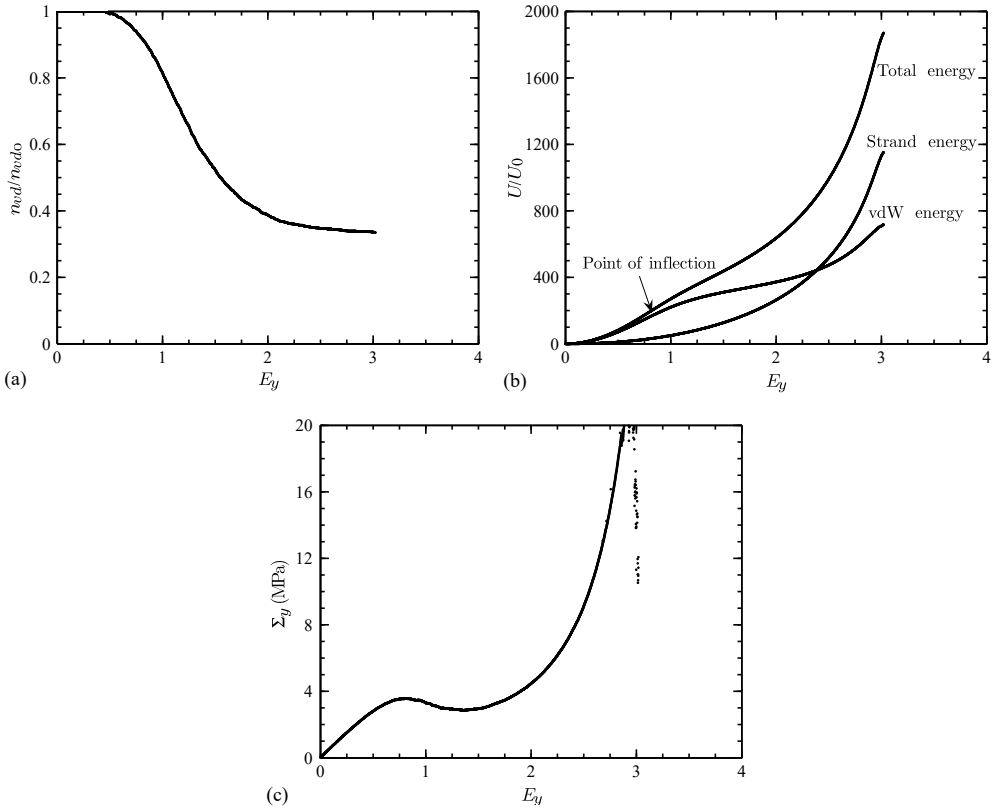


Figure 6. Variation of (a) the number of intact van der Waals bonds n_{vd} as a fraction of the initial number of bonds n_{vd0} , (b) van der Waals, strand and total energies and (c) overall stress Σ_y with imposed strain E_y .

At low strains, the total energy is dominated by the quadratic van der Waals energy. With further straining, the chains begin to stretch and van der Waals bonds also break at the same time. Thus the energy of the strands governed by the inverse Langevin function gains importance. This is also illustrated by the evolution of the individual energy components in figure 6(b). For the parameters chosen for the ‘base’ material, beyond $E_y \approx 2.3$, the energy of the strands dominates the total energy.

Since equation (31) is used to calculate the stress, the point of inflection in the total energy manifests as the yield drop in the overall stress–strain curve shown in figure 6(c). Thus, in this model the yield drop arises due to a changeover in the energetics of deformation from a van der Waals energy dominated situation to a strand energy dominated situation with a large scale breakage of the van der Waals bonds. The qualitatively realistic stress–strain curve obtained from the model exhibits linear elastic behaviour and low strains, softening at yield and finally strain hardening behaviour.

An important point to be noted about figures 6(a) through (c) is the gradual transition in the energetics which leads to a rounded yield drop in the stress–strain curve. The slope change at the point of inflection in the total energy depends on the parameters chosen and especially on the rate at which van der Waals bonds break. A sharp unrealistic drop in stress would result if these bonds broke too quickly.

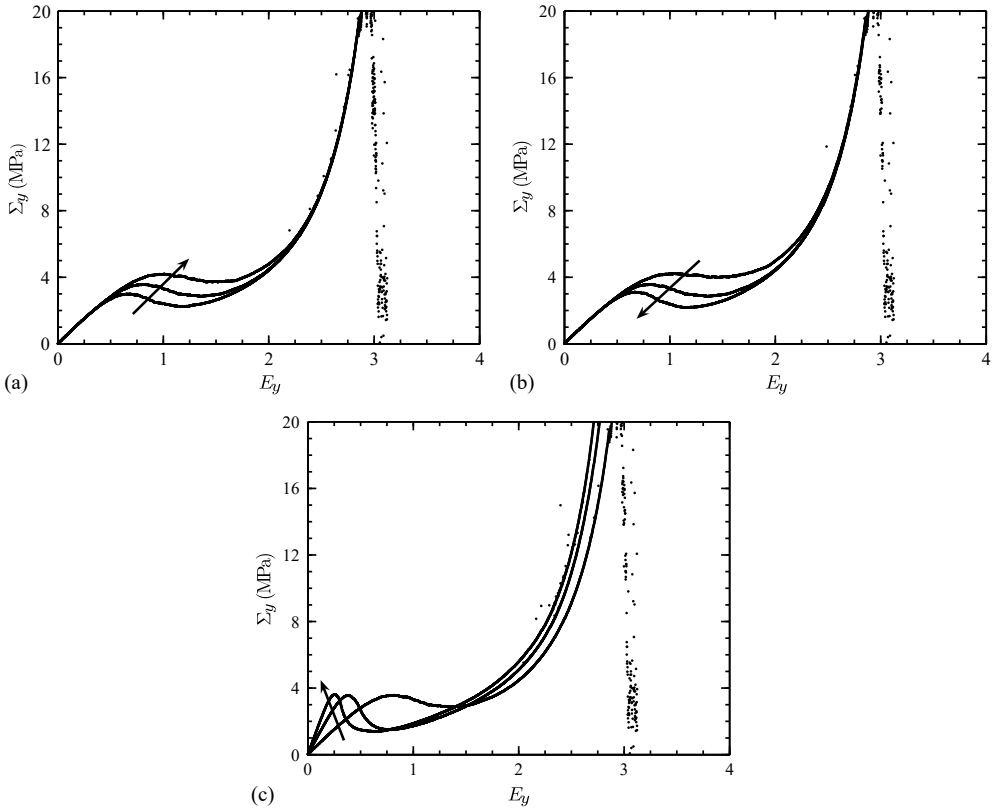


Figure 7. Effects of the values of (a) U_0 , (b) β and (c) K_{vd} on the overall stress (Σ_y) and strain (E_y) response.

The yield drop in solid polymers and its influence on mechanical behaviour has been studied extensively (see, e.g., Lai and van der Giessen (1997), Smit *et al* (2000)). In the TS model, the yield drop comes about as a consequence of a switch in energetics. The severity of the yield drop will consequently depend on the parameters governing van der Waals bond breakage (mainly U_0 and β) vis-a-vis the mechanical properties of the strand (mainly N). It is worth mentioning here that MD studies have shown (see, Negi and Basu (2006)) that the van der Waals energy does flatten with strain after the yield strain. However, further studies are needed to establish whether the physical reason for the yield drop is indeed linked to the early breakage of the van der Waals bonds.

As already discussed, the softening is a consequence of the early breakage of the van der Waals bonds. Thus the pre-softening elastic response is almost entirely dependent on the stiffness of the van der Waals bonds. This is shown in figure 7(c) where the parameter K_{vd} in equation (27) is varied from 4 to 10 MPa. Increasing K_{vd} has the effect of reducing the yield strain while keeping the yield stress almost unchanged. The yield stress is influenced more strongly by the activation energy U_0 and the activation volume β as shown in figures 7(a) and (b). The activation energy U_0 has been varied from 1.8178×10^{-19} to 1.9178×10^{-19} J (i.e. from the original TS values to somewhat higher ones: note that the simulations are very sensitive to the value of U_0). Higher U_0 makes the breaking of van der Waals bonds more difficult leading to a higher yield stress. On the other hand, increasing β makes the breaking of the bonds possible at lower levels of $\hat{\sigma}$ and consequently leads to a lowering of the yield

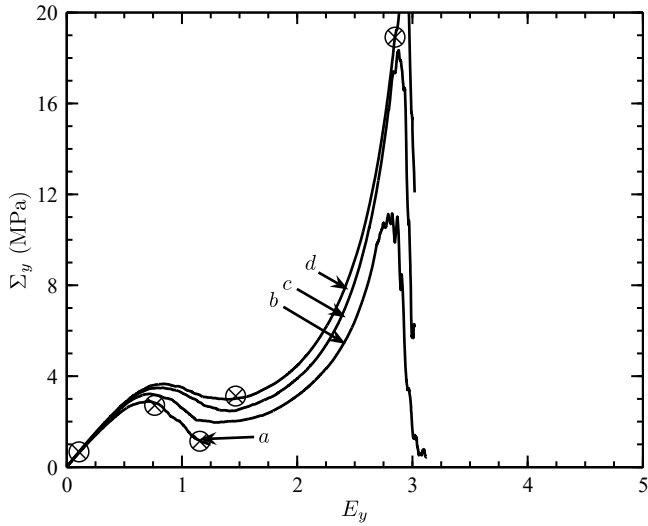


Figure 8. Effect of molecular weight M_w on the overall stress (Σ_y) versus the strain (E_y) response.

stress as shown in figure 7(b).

3.2. Effect of macromolecular and loading parameters

One of the major attractions of a mesoscopic model is that it allows us to connect molecular properties such as molecular weight M_w of polymer chains and the entanglement spacing ϕ to the macroscopic mechanical response. In this section we demonstrate how M_w and ϕ influence the stress–strain response of the polymer. The parameters chosen are identical to that of the ‘base’ material described in the previous section.

A single SARW step roughly corresponds to a chain of $M_w = 1900 \text{ g mol}^{-1}$. We have varied the molecular weight through 1900, 5700, 9500 and 19000. Thus a chain of $M_w = 19000$ corresponds to 10 SARW steps. The overall stress–strain response of all these curves is shown in figure 8. The response is very brittle at $M_w = 1900$ and gradually becomes ductile as M_w increases. This behaviour is quantitatively similar to that observed by Termonia and Smith (1987). The stress–strain behaviour observed in these simulations is also qualitatively similar to the effect of M_w on the ductility observed in experiments (Nunes *et al* 1982). In the experiments, the ultimate elongation as well as the impact strength of high density polyethylene (HDPE) has been shown to increase rapidly with molecular weight till a critical molecular weight of about 5×10^5 was attained. In real polymers, the effect of M_w comes about due to increased intermolecular forces and entanglement effects at high M_w . These effects are mimicked by the TS model successfully.

To systematically examine the effect on the deformation behavior of the entanglement spacing, i.e. of the number of statistical chain segments between entanglements, Termonia and Smith (1988) introduced the spacing factor ϕ defined as

$$\phi = \left(\frac{1900}{M_w} \right), \quad (35)$$

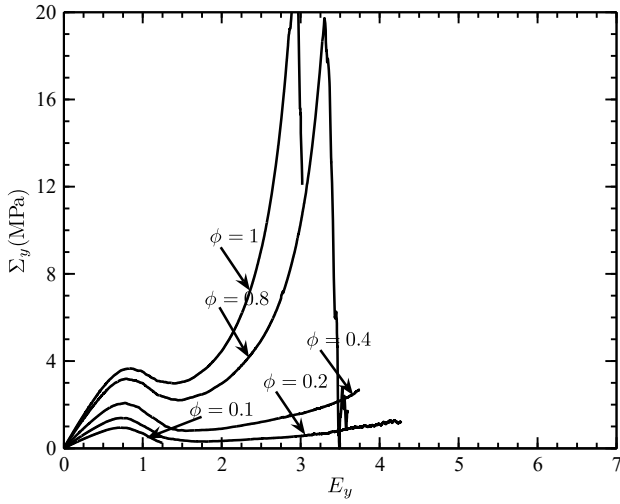


Figure 9. Effect of entanglement spacing ϕ on the overall stress (Σ_y) versus the strain (E_y) response of the base material.

where M_e is the molecular weight between entanglements. The numerical scaling factor 1900 is somewhat arbitrary but pertains to the approximate molecular weight between entanglements in melts of linear polyethylene macromolecules.

Figure 9 shows a series of nominal stress–strain curves calculated for monodisperse polyethylene of $M_w = 19\,000$ at different values of the entanglement spacing factor $\phi = 0.1, 0.2, 0.4, 0.8$ and 1 . A low value of ϕ corresponds to a lightly entangled polymer with strands longer than in linear polyethylene melts, while higher values simulate highly entangled polymers with shorter strands. This figure reveals that the post-yield modulus of highly entangled polymers (large ϕ) is higher than lightly entangled ones. Lightly entangled polymers have an almost perfect plastic response after yielding. Moreover, they bear much lower levels of stress though elongation at failure is somewhat larger for the lightly entangled samples. This again is in keeping with the results obtained by Termonia and Smith (1988) (see, figure 2 of their paper).

Polymers are known to be rate and thermally sensitive and Termonia *et al* (1988) had studied the effects of deformation rate and temperature on the TS model. The essential feature of the rate sensitivity is an increase in the yield stress at high rates of loading. On the other hand, temperature reduces the yield stress and weakens the hardening process. The weakening of the hardening response is due to thermally activated loss of entanglements (see Raha and Bowden (1972), Arruda *et al* (1993)). According to Raha and Bowden (1972), the density of strands obeys

$$n_s(T) = B - D \exp\left(-\frac{E_a}{RT}\right), \quad (36)$$

where E_a and D are constants. Moreover since the total number of monomers in the ensemble is constant, $n_s N$ is fixed. This leads to the fact that the number of Kuhn segments between entanglements at temperatures T_1 and T_2 follows the relation

$$\frac{N_2}{N_1} = \frac{1 - \frac{D}{B} \exp\left(-\frac{E_a}{RT_1}\right)}{1 - \frac{D}{B} \exp\left(-\frac{E_a}{RT_2}\right)}. \quad (37)$$

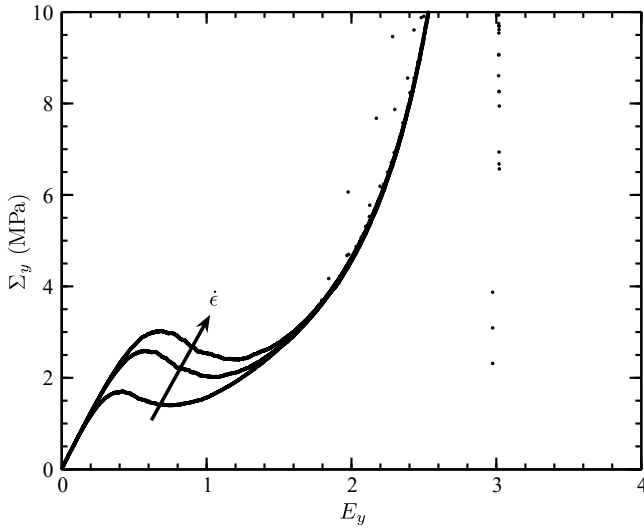


Figure 10. Overall stress (Σ_y) versus strain (E_y) responses at deformation rates of \dot{E}_y of 1, 5 and 10 min^{-1} for the base material.

Following Basu and van der Giessen (2002) we have taken $D/B = 1.648 \times 10^3$ and $E_a/R = 2.8 \times 10^3 \text{ K}$ in this work.

Figure 10 shows the effect of the strain rate on the stress–strain response of the ‘base’ material. The overall strain rates (i.e. rate of change in E_y) used are $\dot{E}_y = 1, 5$ and 10 min^{-1} . As expected, the material hardens with strain rate and, in particular, the yield stress increases with the increase in rate. In the TS model, the rate sensitivity arises from equation (32) which governs the breakage of the van der Waals bonds. This is illustrated in figure 11 where the fraction of the intact van der Waals bonds n_s with respect to the initial number n_{s0} is plotted at various rates. At higher rates, owing to the short times involved in the deformation, larger number of van der Waals bonds survive large deformations allowing the material to carry higher stresses. Also note that the hardening response is not dependent on the deformation rate. In the TS model, the rate insensitivity of the large strain behaviour is due to the fact that most of the load at large strains is borne by strands which are governed by the rate-insensitive inverse Langevin function. This feature of the model is not entirely consistent with experimental results where the stress–strain curves are seen to shift upwards almost parallel to each other with the deformation rate (see, e.g., G’Sell and Gopez (1981)).

Figure 12 shows the effect of temperature on the stress–strain response. At every temperature the number of Kuhn segments is adjusted according to equation (37). The large strain behaviour of the polymer at high temperatures is similar to that for low ϕ as in figure 8. This is not surprising since high temperatures lead to a larger number of Kuhn segments between entanglements.

Another interesting effect of high temperature is the change in the yield drop as the temperature changes. It should be noted that continuum models of polymers (e.g. Boyce *et al* 1988, Wu and van der Giessen 1993) do not capture the change in yield drop with temperature. However, change in the yield drop with temperature is seen in experimental studies as in the work of G’Sell and Gopez (1981). In this model, both the rate of breakage of the van der Waals bonds and the force stretch relationship of the strands depend on T . Thus the energetics of the van der Waals bond stretching as well as chain deformation are altered

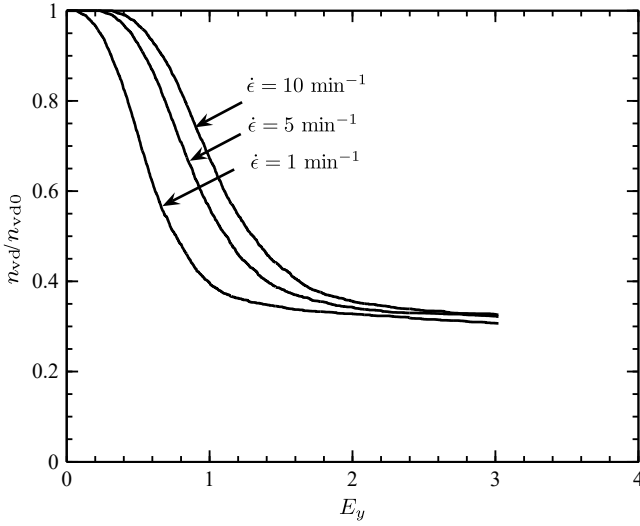


Figure 11. Evolution of the fraction of the intact bonds (n_{vd}/n_{vd0}) with strain (E_y) at the same deformation rates as in figure 10.

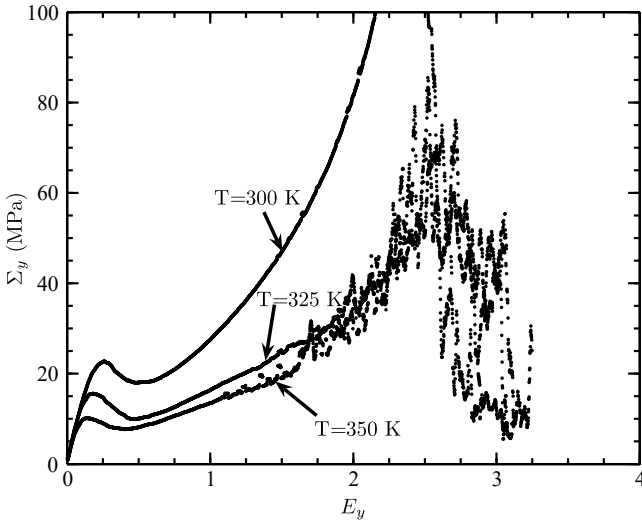


Figure 12. Stress (Σ_y) and strain (E_y) responses of the polymer at different temperatures T as predicted by the TS model.

with temperature. For example, at 325 K a higher difference between the van der Waals energy and the energy of the strands at the yield point leads to a larger yield drop.

In summary, the above discussion reinforces the fact that the TS model is a viable mesoscale model for polymer deformation as it has intrinsic capability of capturing many of the essential features of the stress–strain response of polymers. These include the yield drop, the post-yield hardening response and the thermal sensitivity. However, in the present form rate sensitivity of these materials is not properly represented by the model.

The stress–strain responses shown in figures 8 and 9 match closely with the original results of Termonia and Smith (1987, 1988). This implies that the model formulated in this

paper works as well as the original model proposed by Termonia and Smith (1987). However, the present approach systematically positions the method within the framework of the finite element method, the generality of which is firmly established. The results pertaining to the strain rate and thermal sensitivity of polymers are also realistic.

4. Conclusions

In this work, the Termonia and Smith (1987, 1988) model has been analysed critically. The primary objective is to ascertain the applicability of this mesoscopic model to predicting the mechanical response of polymers. The implementation of the model has been clearly explained, in our opinion, to an extent not done in the previous literature. The model has been implemented within the framework of the large deformation based finite element method wherein the two-dimensional lattice is viewed as a non-linear truss assemblage.

We have highlighted an important physical basis of the model, namely, that it implicitly assumes a switch in the energetics of deformation from being governed by the non-bonded van der Waals forces at low strains to the intrachain forces at higher strains. The parameters in the model basically tend to influence the competition between these two energies. The yield drop in the stress–strain response is a significant consequence of the switch in energetics. The post-yield hardening response of the polymer is on the other hand a consequence of the inverse Langevin nature of the strand response.

We have also looked at the significance of each parameter in the TS model and have shown that particular salient features in the stress–strain response of glassy polymers such as the elastic modulus, yield stress, yield drop and hardening are primarily governed by particular parameters in the model. A qualitative description of the stress–strain behaviour at low strain rates is thus given by the TS model.

Acknowledgments

One of the authors (SB) acknowledges the funding received for this work from the Department of Science and Technology, Government of India, through Project Number SR/S2/CMP-35/2003.

References

- Arruda E M, Boyce M C and Jayachandran R 1993 Effects of strain rate, temperature and thermomechanical coupling on the finite strain deformation of glassy polymers *Mech. Mater.* **19** 193–212
- Basu S and van der Giessen E 2002 A thermo-mechanical study of mode: I. Small scale yielding crack-tip fields in glassy polymers *Int. J. Plast.* **18** 1395–423
- Bicerano J, Grant N K, Seitz J T and Pant K 1997 Microstructural model for prediction of stress–strain curves of amorphous and semicrystalline elastomers *J. Polym. Sci.* **35** 2715–36
- Boyce M, Parks D M and Argon A S 1988 Large inelastic deformation of glassy polymers: 1. Rate dependent constitutive model *Mech. Mater.* **7** 15–33
- Brown D and Clarke J H R 1991 Molecular dynamics simulation of an amorphous polymer under tension: 1. Phenomenology *Macromolecules* **24** 2075–82
- Capaldi F M, Boyce M C and Rutledge G C 2004 Molecular response of a glassy polymer to active deformation *Polymer* **45** 1391–9
- Curtin W A and Scher H 1990 Mechanics modelling using a spring network *J. Mater. Res.* **5** 554–62
- Curtin W A and Pamel M 1997 Time-dependent damage evolution and failure in materials: II. Simulations *Phys. Rev. B* **55** 12051–61
- Gonzalez C and Llorca J 2003 A numerical model to simulate the deformation and fracture of polyethylene fibres *Modelling Simul. Mater. Sci. Eng.* **11** 349–64

- G'Sell C and Gopez A J 1981 Plastic banding in glassy polycarbonate under plane simple shear *J. Mater. Sci.* **20** 3462–78
- Heymans N 1988 Radius of gyration, maximum extensibility and intrinsic crazing in thermoplastics *J. Mater. Sci.* **23** 2394–402
- Jagota A and Bennison S J 1995 Element breaking rules in computational models for brittle fracture *Modelling Simul. Mater. Sci. Eng.* **3** 485–501
- Lai J and van der Giessen E 1997 A numerical study of crack-tip plasticity in glassy polymers *Mech. Mater.* **25** 183–97
- Mansfield M L 1982 Monte Carlo studies of polymer chain dimensions in the melt *J. Chem. Phys.* **77** 1554–9
- Meirovitch H 1987 A new simulation of branched polymers *J. Phys. A: Math. Gen.* **20** 6057–73
- Negi A and Basu S 2006 A molecular dynamics study of the strength and ductility of high T_g polymers *Modelling Simul. Mater. Sci. Eng.* **14** 563–80
- Nunes R W, Martin J R and Johnson J F 1982 Influence of molecular weight and molecular weight distribution on mechanical properties of polymers *Polym. Eng. Sci.* **22** 205–28
- Perrin G 2000 Analytic stress–strain relationship for isotropic model of rubber elasticity *C. R. Acad. Sci. Paris* **328** 5–10
- Raha S and Bowden P B 1972 Birefringence of plastically deformed poly(methyl methacrylate) *Polymer* **13** 174–83
- Smit R J M, Brekelmans W A M and Meijer H E H 2000 Predictive modelling of the properties and toughness of polymeric materials: I. Why is polystyrene brittle and polycarbonate tough? *J. Mater. Sci.* **35** 2855–67
- Sokal A D 1995 Monte Carlo methods for the self-avoiding random walk *Monte Carlo and Molecular Dynamics Simulations in Polymer Science* ed K Binder (London: Oxford University Press)
- Termonia Y and Smith P 1987 Kinetic model for tensile deformation of polymers: effect of molecular weight *Macromolecules* **20** 835–8
- Termonia Y and Smith P 1988 Kinetic model for tensile deformation of polymers: effect of entanglement spacing *Macromolecules* **20** 2184–9
- Termonia Y, Allen S R and Smith P 1988 Kinetic model for tensile deformation of polymers: 3. Effects of deformation rate and temperature *Macromolecules* **21** 3485–9
- Terzis A F, Theodorou D N and Stroeks A 2002 Entanglement network of the polypropylene/polyamide interface: 3. Deformation to fracture *Macromolecules* **35** 508–21
- Treloar L R G 1975 *Physics of Rubber Elasticity* (London: Oxford University Press)
- Vujosevic M and Krajcinovic D 1997 Creep rupture of polymers—a statistical model *Int. J. Solids Struct.* **34** 1105–22
- Washiyama J, Kramer E J and Hui C-Y 1993 Fracture mechanisms of polymer interfaces reinforced with block copolymers: transition from chain pullout to crazing *Macromolecules* **26** 2928–34
- Wu P D and Van der Giessen E 1993 On improved network models for rubber elasticity and their applications to orientation hardening in glassy polymers *J. Mech. Phys. Solids* **41** 427–56